

Systematic R -matrix analysis of the $^{13}\text{C}(p, \gamma)^{14}\text{N}$ capture reaction

Suprita Chakraborty,¹ Richard deBoer,² Avijit Mukherjee,¹ and Subinit Roy^{3,*}

¹*Department of Physics, Jadavpur University, Kolkata 700032, India*

²*University of Notre Dame, Notre Dame, Indiana 46556, USA*

³*Saha Institute of Nuclear Physics, 1/AF, Bidhan Nagar, Kolkata 700064, India*

(Received 10 October 2014; revised manuscript received 27 February 2015; published 1 April 2015; corrected 24 April 2015)

Background: The proton capture reaction $^{13}\text{C}(p, \gamma)^{14}\text{N}$ is an important reaction in the CNO cycle during hydrogen burning in stars with mass greater than the mass of the Sun. It also occurs in astrophysical sites such as red giant stars: the asymptotic giant branch (AGB) stars. The low energy astrophysical S factor of this reaction is dominated by a resonance state at an excitation energy of around 8.06 MeV ($J^\pi = 1^-, T = 1$) in ^{14}N . The other significant contributions come from the low energy tail of the broad resonance with $J^\pi = 0^-, T = 1$ at an excitation of 8.78 MeV and the direct capture process.

Purpose: Measurements of the low energy astrophysical S factor of the radiative capture reaction $^{13}\text{C}(p, \gamma)^{14}\text{N}$ reported extrapolated values of $S(0)$ that differ by about 30%. Subsequent R -matrix analysis and potential model calculations also yielded significantly different values for $S(0)$. The present work intends to look into the discrepancy through a detailed R -matrix analysis with emphasis on the associated uncertainties.

Method: A systematic reanalysis of the available decay data following the capture to the $J^\pi = 1^-, T = 1$ resonance state of ^{14}N around 8.06 MeV excitation had been performed within the framework of the R -matrix method. A simultaneous analysis of the $^{13}\text{C}(p, p_0)$ data, measured over a similar energy range, was carried out with the capture data. The data for the ground state decay of the broad resonance state ($J^\pi = 0^-, T = 1$) around 8.78 MeV excitations was included as well. The external capture model along with the background poles to simulate the internal capture contribution were used to estimate the direct capture contribution. The asymptotic normalization constants (ANCs) for all states were extracted from the capture data. The multichannel, multilevel R -matrix code AZURE2 was used for the calculation.

Results: The values of the astrophysical S factor at zero relative energy, resulting from the present analysis, are found to be consistent within the error bars for the two sets of capture data used. However, it is found from the fits to the elastic scattering data that the position of the $J^\pi = 1^-, T = 1$ resonance state is uncertain by about 0.6 keV, preferring an excitation energy value of 8.062 MeV. Also the extracted ANC values for the states of ^{14}N corroborate the values from the transfer reaction studies. The reaction rates from the present calculation are about 10–15% lower than the values of the NACRE II compilation but compare well with those from NACRE I.

Conclusion: The precise energy of the $J^\pi = 1^-, T = 1$ resonance level around 8.06 MeV in ^{14}N must be determined. Further measurements around and below 100 keV with precision are necessary to reduce the uncertainty in the S -factor value at zero relative energy.

DOI: [10.1103/PhysRevC.91.045801](https://doi.org/10.1103/PhysRevC.91.045801)

PACS number(s): 25.60.Bx, 24.10.Ht, 25.40.Lw, 27.20.+n

I. INTRODUCTION

The $^{13}\text{C}(p, \gamma)^{14}\text{N}$ reaction is a key reaction in the CNO cycle, a sequence of reactions that dominates the energy production in the hydrogen-burning stage of stars that have masses greater than the solar mass [1]. It occurs in different astrophysical sites, e.g., the red giants, asymptotic giant branch (AGB) stars, in the effective temperature range of $T = 0.03\text{--}0.1$ GK. In AGB stars, the reaction $^{13}\text{C}(\alpha, n)^{16}\text{O}$ is one of the source reactions generating free neutrons for subsequent nucleosynthesis through the slow neutron capture process. The capture reaction $^{13}\text{C}(p, \gamma)^{14}\text{N}$ depletes the seed nucleus ^{13}C for the reaction $^{13}\text{C}(\alpha, n)$ in AGB stars of solar metallicity [2]. The reaction is also important for estimating the abundance ratio $^{12}\text{C}/^{13}\text{C}$, an observable for the chemical composition of surface layers of stars, and a measure of subsequent stellar evolution and nucleosynthesis [1,3,4].

The low energy cross section $\sigma(E)$ or the astrophysical S factor $S(E)$ of the radiative capture reaction $^{13}\text{C}(p, \gamma)^{14}\text{N}$ ($Q = 7.551$ MeV) [5] is dominated by an s -wave resonance with $J^\pi = 1^-$ and $T = 1$ around the excitation energy of 8.06 MeV in the nucleus ^{14}N . This state has been observed to decay to seven low-lying bound states of ^{14}N [6]. Another s -wave resonance with $J^\pi = 0^-$ and $T = 1$ around 8.78 MeV excitation in ^{14}N , a broad resonance of width ~ 400 keV and decaying to four of the low-lying states of ^{14}N , is also expected to affect the low energy cross sections of the capture reaction. Along with the direct capture process, these two resonant processes determine the $^{13}\text{C}(p, \gamma)^{14}\text{N}$ capture reaction rate at astrophysically relevant energies. The narrow d -wave resonance of $J^\pi = 2^-$ at an excitation energy of 7.97 MeV does not have any significant contribution at energies of astrophysical interest.

The capture reaction $^{13}\text{C}(p, \gamma)^{14}\text{N}$ has been studied over a wide range of proton beam energies [6–11]. The cross section measurement was extended down to a beam energy of about 100 keV. Prior to the work of King *et al.* [6], the measurements

*subinit.roy@saha.ac.in

were restricted to the cross section for the decay to the ground state of ^{14}N [9,10]. Based on these data and with a correction of 18% [12] for cascade transitions, the recommended value of the astrophysical S factor at zero energy was 5.5 keV b [13]. A systematic measurement of $^{13}\text{C}(p,\gamma)^{14}\text{N}$ capture reaction data over $E_p(\text{lab}) = 120\text{--}950$ keV by King *et al.* [6] yielded, on extrapolation to stellar energies, astrophysical S -factor values of $S(0) = 7.64$ keV b at $E_{\text{c.m.}} = 0$ and $S(25) = 7.7 \pm 1.0$ keV b at $E_{\text{c.m.}} = 25$ keV. The estimated values included the explicit contributions of primary decays from the resonances to the low-lying excited states of ^{14}N in addition to decay to the ground state. The value obtained by King *et al.* differed from the previously recommended value of $S(0) = 5.5$ keV b [13]. Mukhamedzhanov *et al.* [14] carried out a reanalysis of the data of King *et al.* within the R -matrix framework, using the spectroscopic information of $^{13}\text{C} + p$ and ^{14}N overlaps from the peripheral transfer reaction studies. The resultant $S(0) = 7.6 \pm 1.1$ keV b corroborated the value obtained by King *et al.* [6]. A recently reported measurement, in reverse kinematics, of the cross section of the decay of the 8.062 MeV resonance state to the ground state of ^{14}N and a subsequent R -matrix analysis of the data provided $S(0) = 4.85 \pm 0.76$ keV b [11]. The value is again significantly lower than that of Refs. [6,14] but matched well with the values given in Ref. [13]. The difference, as has been conjectured in Refs. [6,14], comes probably from the inadequate estimation of contributions to the value of $S(0)$ from the decays to the excited states of ^{14}N . However, we note that even the contributions to total $S(0)$ from the decay to the ground state differ significantly in the measurements of Refs. [6,11]. Absolute normalization of the cross section data could also be a possible source of discrepancy. This should be probed further.

In this context, we present a systematic reanalysis of the capture data of King *et al.* and Genard *et al.* for the resonance state ($J^\pi = 1^-, T = 1$) at around 8.062 MeV. In the energy range $E_{\text{c.m.}} < 100$ keV, where no measurement exists, the cross section or astrophysical S factor for the $^{13}\text{C}(p,\gamma)^{14}\text{N}$ reaction has a significant nonresonant contribution from the direct capture process and the tail of the broad resonance around 8.776 MeV excitation. To make a more constrained analysis, we performed a simultaneous fit to the data for the decay of the broad resonance ($J^\pi = 0^-, T = 1$) around 8.776 MeV to the ground state of ^{14}N and the elastic scattering excitation function data at two different angles in addition to the decay data for the resonance at 8.062 MeV excitation. The higher energy resonance data were taken from Ref. [15]. The $^{13}\text{C} + p$ elastic scattering data of Hebbard *et al.* [9] over the center-of-mass energy range of 200 to 700 keV at 90° and 120° were included in the analysis scheme. The global fitting was performed within the R -matrix formalism using the multichannel, multilevel R -matrix code AZURE2 [16]. The alternate R -matrix parametrization of Ref. [17] has been used in the present analysis.

The details of the analysis are described in Sec. II. The results—including the contributions from resonant and direct capture processes along with the component due to interference of the two amplitudes, the total S -factor value, and the associated uncertainties—are given in Sec. III. It

also includes the resultant reaction rates obtained from the calculation. Finally, the work is summarized in Sec. IV.

II. ANALYSIS

In the determination of the astrophysical S factor at zero energy for proton capture on ^{13}C , two of the resonances of ^{14}N above the $^{13}\text{C} + p$ threshold make significant contributions to the cross section besides the nonresonant capture reaction. The resonance ($J^\pi = 1^-, T = 1$) (subsequently referred to as R2) located around $E_{\text{c.m.}} = 511.0 \pm 1.0$ keV [5] plays the most dominant role in the extrapolation of the cross section to stellar energies. In Ref. [6], this resonance is positioned at $E_{\text{c.m.}} = 518$ keV. The other resonance that contributes to the value of $S(0)$ is a broad resonance ($J^\pi = 0^-, T = 1$) (henceforth referred to as R5) at $E_{\text{c.m.}} = 1225.0 \pm 7.0$ keV [5,18] with a width of ~ 400 keV. The resonance R2 decays primarily to the ground state and the first five excited states of ^{14}N while the resonance R5 decays to the ground and three of the excited states of the final nucleus [19]. All these decays contribute to form the resonant component of the total S -factor value. The ground state and the first two excited states in ^{14}N are negative parity states, hence the transitions from the two resonances are $E1$ in nature. The transitions to other excited states in consideration are either $M1$ or $E2$ type transitions. The scenario of important resonant decays, considered for the present R -matrix analysis, is schematically shown in Fig. 1. The decays to the ground and the first six excited states of ^{14}N following the nonresonant capture occur predominantly through $E1$ transitions. Consequently, there can be interference between the resonant and nonresonant amplitudes of transitions to the first three positive parity states of the ^{14}N nucleus. The S factors corresponding to the transitions to negative parity excited states are the incoherent sum of resonant and nonresonant contributions. To start with, we reanalyzed the data measured and reported by King *et al.* [6] for the decays of the resonant state ($1^-, 1$) of ^{14}N at $E_{\text{c.m.}} = 511.0 \pm 1.0$ keV and available from the EXFOR database [20]. The decay to the sixth excited state of ^{14}N , for which the data is not sufficient, is not considered in the fitting routine of the analysis.

In the R -matrix theory, the *channel radius* (r_c) divides the coordinate space into an external part and an internal part [21]. Accordingly, the (p,γ) capture cross section is divided into an external capture contribution coming from the radial region beyond r_c and an internal capture contribution from the region below r_c [16]. The direct or nonresonant component of the external capture contribution is estimated following the external capture model described in Refs. [16,22,23]. The magnitude of the external capture cross section, which has a given energy dependence, is determined by the *asymptotic normalization coefficient* (ANC) of the final bound state [23]. The internal capture component of the direct or nonresonant contribution, on the other hand, is simulated by the high energy background poles. Thus the direct capture part of the cross section is modeled as a sum of external capture model and the high energy background poles in AZURE2. The channel radius, r_c , in the present calculation was fixed at

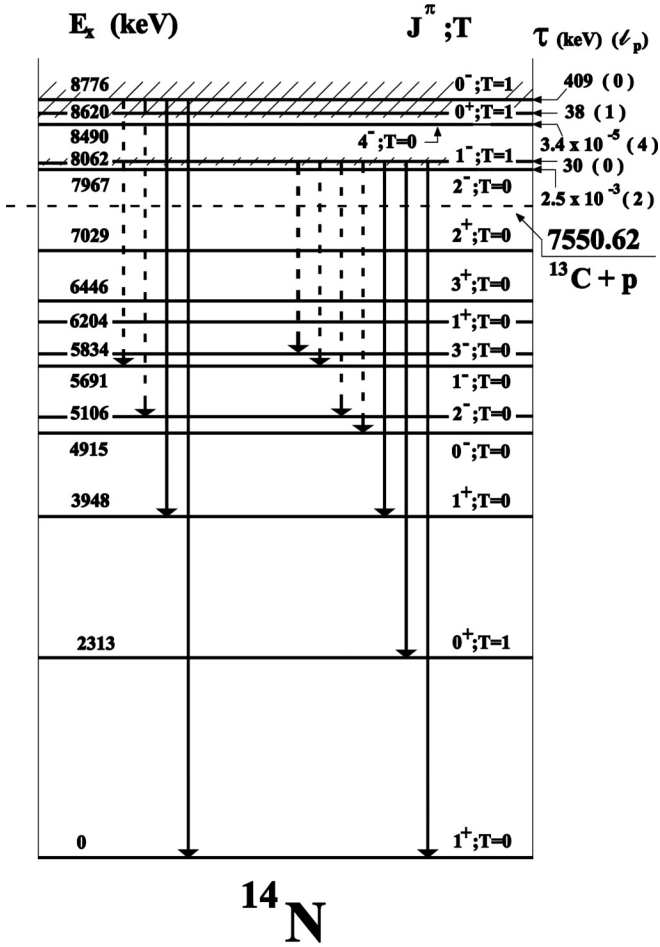


FIG. 1. Level scheme of ^{14}N from Ref. [18]. The vertical arrows denote the transitions considered in the R -matrix calculation. The solid arrows indicate $E1$ transitions while the dashed arrows indicate $M1/E2$ transitions.

$r_c = r_0 \times (A_p^{1/3} + A_T^{1/3}) = 4.19$ fm with $r_0 = 1.25$ fm following the systematic (p, γ) capture reaction analysis of Ref. [24].

A. Asymptotic normalization coefficients

The asymptotic normalization coefficient or ANC defines the magnitude of the tail of the two-body bound state wave function of the target plus projectile in the composite nucleus. It is related to the spectroscopic factor of the bound state of the final nucleus by the relation

$$C^2 S_{J_f l_f} = \left(\frac{C_{J_f l_f}}{b_{l_f j_f}} \right)^2, \quad (1)$$

where $C^2 S_{J_f l_f}$ is the spectroscopic factor of the final bound state of the composite nucleus with spin J_f . The relative orbital angular momentum and spin between the two clusters in the composite are denoted by l_f and j_f . The factor C^2 denotes the square of the isospin Clebsch-Gordon coefficient. $C_{J_f l_f}$ is the corresponding ANC and $b_{l_f j_f}$ is the single-particle asymptotic normalization constant with l_f and j_f quantum numbers of the orbital. ANCs can be used as free parameters

TABLE I. The ANCs for $^{13}\text{C}(p, \gamma)^{14}\text{N}$ determined from the capture data of Ref. [6]. Columns 4 and 5 list the ANCs resulted from χ^2 minimization without and with the high energy background poles. Column 6 gives the uncertainty associated with each ANC value of column 5 corresponding to $\chi^2 = \chi_{\min}^2 + 1$. The lower and upper limits of uncertainties in ANC values extracted from transfer data [14] are shown in the last column (column 7) for comparison.

Energy (J^π) (MeV)	L	S	ANC (Without bg pole) ($\text{fm}^{1/2}$)	ANC (With bg pole) ($\text{fm}^{1/2}$)	ANC range (from fit) ($\text{fm}^{1/2}$)	ANC (lit.) ^a ($\text{fm}^{1/2}$)
0.0 (1^+)	1	0	1.977	1.370	1.10–1.74	1.565–1.807
	1	1	1.775	3.986	3.11–4.20	3.988–4.075
2.31 (0^+)	1	1	3.318	2.974	2.05–3.76	2.828–3.130
3.95 (1^+)	1	0	0.808	0.851	0.80–0.87	0.950–1.008
	1	1	1.008	1.235	0.90–1.27	1.344–1.426
4.92 (0^-)	0	0	5.258	6.025	5.03–6.28	5.403–6.067 ^b
5.11 (2^-)	2	0	0.743	0.690	0.21–0.77	0.471–0.508
	2	1	0.006	0.340	0.16–0.55	0.385–0.415
5.69 (1^-)	1	0	6.041	4.706	4.60–6.97	3.309–3.324

^aANCs are given in JJ coupling scheme in Ref. [14].

^b $C^2 = 33.00 \pm 3.81$ fm^{-1} from Table 3, Ref. [14] has been used to estimate the limits.

in fitting the capture reaction data or they can be kept fixed at values determined from the relevant transfer reaction data.

To fix the ANCs to be used in the present analysis, we followed the prescription of Ref. [25]. In the first step, we performed a simultaneous fitting of the primary capture data of King *et al.* [6] and the scattering data of Hebbard *et al.* [9] without introducing any background poles. The ANCs were left as free parameters for χ^2 minimization and the ANCs resulted are listed in the fourth column of Table I. Next the high energy background poles were introduced, which were supposed to take care of the internal capture contribution of the direct capture component. The high energy s -wave background poles were placed at 15 MeV excitation energy, about 8 MeV above the highest excitation energy considered in the calculation. The particle widths of these states were taken to be $\Gamma_p = 5$ MeV, a value close to the Wigner limit [1], Γ_w , corresponding to the chosen channel radius of 4.19 fm. The gamma widths Γ_γ were left as fit parameters. Again a χ^2 minimization routine was performed. Column 5 displays the ANCs obtained with minimum χ^2 when background poles were introduced for all the transitions. The ANC values of columns 4 and 5 were then compared with the values obtained by Mukhamedzhanov *et al.* [14] who used the data of the one-proton stripping reactions, $^{13}\text{C}(^3\text{He}, d)^{14}\text{N}$ and $^{13}\text{C}(^{14}\text{N}, ^{13}\text{C})^{14}\text{N}$ [26,27], to extract the ANCs.

The comparison with the literature values indicates that significant improvement in the ANC values occurred not only for the ground state but also for the excited states with the introduction of the background poles. The ANC values resulting from the simultaneous fitting of the capture data and the elastic scattering data, and corresponding to the minimum χ^2 values, are quite close to the values obtained from the transfer reaction studies. It is evident that the captures to

the states of the strongly bound nucleus ^{14}N have dominant contributions from the internal capture part simulated by the high energy background poles. The chosen ANC values essentially generate the external capture component of the direct capture cross section. Subsequent to the fixing of the ANC values to be used (column 5) in the present analysis, a calculation was performed to obtain the range of each ANC value corresponding to $\chi^2 = \chi_{\min}^2 + 1$. The range associated with each ANC is displayed in the column 6 of the table. The broader range associated with the ANC from the capture reaction data, compared to that obtained from the transfer reaction study (column 7), clearly shows that the ANC values are not so strongly restricted by the radiative capture data. However, we have used the ANC values resulting from our analysis, and an uncertainty term in the S factor of an individual transition has been introduced corresponding to the limits of the associated ANC value.

B. Simultaneous fitting

Two different data sets were constructed for the simultaneous fitting procedure. *Data Set I* consisted of the data of King *et al.* [6] for resonance R2, the data of Zeps *et al.* [15] for the ground state decay of resonance R5, and the elastic scattering data of Hebbard *et al.* [9] at $\theta_{\text{lab}} = 90^\circ$ and 120° . *Data Set II*, on the other hand, consisted of the capture data of Genard *et al.* [11] for the decay of R2 to the ground state of ^{14}N , the data of Zeps *et al.*, the high energy tail part of the ground state decay of the resonance R2 from the data of King *et al.* [6], and the scattering data of Ref. [9]. The simultaneous fit to Data Set I was then carried out using the ANC values listed in column 5 of Table I. The background pole energies and particle widths (Γ_p), shown in Table II, were kept fixed during the search. The best fit resonance parameters are listed in the upper half of Table II. The fitted values for the gamma widths (Γ_γ) of background poles are also shown in Table II. These values are larger than the values used in Ref. [14] but are consistent with the Weiskopff limit for the corresponding gamma energy [1]. A similar fitting procedure was followed for Data Set II as well. The lower half of Table II displays the parameters obtained through the global fit to Data Set II. The ANC values, the energies and the particle widths of the background poles were kept fixed. The excitation energy, Γ_p ,

TABLE II. The resonance parameters obtained from the R matrix fits to the two data sets used in the analysis. Uncertainties in the parentheses do not include the overall normalization uncertainty in the data.

	E_x (MeV)	Γ_p (keV)	J^π	Γ_γ (eV)					
				$R \rightarrow 0.0$	$R \rightarrow 2.31$	$R \rightarrow 3.95$	$R \rightarrow 4.92$	$R \rightarrow 5.11$	$R \rightarrow 5.69$
Data Set I	8.068(3)	37.17(30)	1^-	9.087(50)	0.218(40)	1.544(9)	0.262(10)	0.074(8)	0.612(6)
	8.801	460	0^-	40.96		0.556		0.230	0.230
	15.0	5000	0^-	4.54×10^3		9.53×10^3		2.92×10^3	10×10^3
	15.0	5000	1^-	5.61×10^3	6.42	7.79×10^3	526.1	82.9	960.0
Data Set II	8.062(3)	36.00(28)	1^-	8.11(4)					
	8.801	460	0^-	40.96					
	15.0	5000	0^-	4.54×10^3					
	15.0	5000	1^-	4.46×10^3					

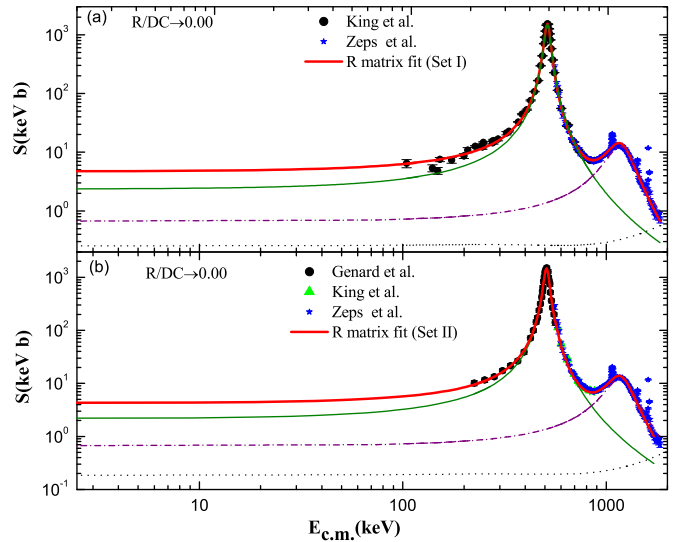


FIG. 2. (Color online) R -matrix fit to the $S(E)$ data for the $R, DC \rightarrow 0.00$ transition. The solid red line gives the total $S(E)$ for this transition and solid green line gives the contribution from resonance R2. The dashed-dotted line describes the R5 resonant component while the dotted line describes the direct capture component. (a) shows the fit to Data Set I and (b) the fit to Data Set II (see text).

and Γ_γ of resonance R5 obtained from the fit to Data Set I were kept unchanged in the fitting of Data Set II.

III. RESULTS AND DISCUSSION

A. Transition to ground state

The resultant fit to the astrophysical $S(E)$ of the $R, DC \rightarrow 0.0$ ($J^\pi = 1^+$, $T = 0$) transition is shown in Fig. 2(a). The thick red solid line in the figure shows the total $S(E)$ from the R -matrix fit. The individual contributions from the resonances R2 and R5 and the direct capture process have also been shown in the diagram. Obviously, the 1^- resonance R2 at 8.068 MeV has the most dominant contribution to the cross sections at the extrapolated energy region. The direct capture contribution to the ground state transition is smaller than both the resonant contributions at $E = 0$. The fit, on extrapolation, provides $S(0) = 4.72 \pm 0.66$ keV b, with individual resonant

and direct capture contributions being $S^{R2}(0) = 2.35$ keV b, $S^{R5} = 0.65$ keV b, and $S^{dc}(0) = 0.25$ keV b. The uncertainty in the $S(0)$ here does not include the uncertainty due to the 11.3% systematic error. The interference between the resonant and direct capture amplitudes constitutes about 31% of the total $S(0)$ for this transition with $S^{\text{int}}(0) = 1.46$ keV b. The $S(0)$ value obtained for Data Set I is less than the value of 5.16 ± 0.71 keV b in Ref. [14] but is consistent within the error bar.

Data Set II was subsequently fitted with AZURE2. The resulting curve, shown in Fig. 2(b), generates the high energy tail of resonance R2 quite nicely, where the data points were taken from Ref. [6]. It also reproduces the R5 data of Zeps *et al.* [15]. The extrapolated value of $S(E)$ at $E_{\text{c.m.}} = 0$ for Data Set II with the parameters of Table II is 4.23 ± 0.67 keV b and the resonant contributions from R2 and R5 are 2.16 keV b and 0.65 keV b respectively. The direct capture contribution is found to be 0.18 keV b while the interference component is 1.24 keV b. Overall the two data sets yield comparable $S(0)$ values for the ground state transition, contrary to the observation of Ref. [11].

Two things are to be noted from the present analysis regarding the parameters of resonance R2. First, the width of resonance R2, obtained from the fit to Data Set I, is comparable with the value obtained from fitting Data Set II. The values agree well with those given in Refs. [6,15]. Second is the reproduction of the elastic scattering data of Hebbard *et al.* [9] by the two sets of resonance parameters. Both the parameter sets reproduce the elastic scattering data in the lower and the higher energy regions dominated by Rutherford scattering away from the resonance. However, at the scattering anomaly region on the resonance, the parameter set (Set 2) with $E_r = 511.4$ keV and particle width $\Gamma_p = 36$ keV from Data Set II produces a remarkably good fit to the elastic data. The excitation function curve (dashed curve) generated with the parameter set (Set 1) obtained from the fit to Data Set I clearly shows a shift in this region. The fits to the elastic scattering excitation functions at the angles 90° and 120° with two sets of parameters are shown in Fig. 3. In Fig. 4, the low energy fall-off of the astrophysical S factor for $^{13}\text{C}(p,\gamma)^{14}\text{N}_{\text{gs}}$ reaction predicted by the R -matrix analysis with the two sets of parameters, Sets 1 and 2, has been shown in comparison with the available experimental data from Refs. [6,7,9–11].

B. Transition to excited states

The reproductions of the energy dependence of the astrophysical S factor, $S(E)$, for the transitions to the excited states of ^{14}N from the R -matrix calculation are shown in Figs. 5 and 6. The $S(E)$ for $R/DC \rightarrow 2.31$ MeV [Fig. 5(a)] and $R/DC \rightarrow 4.92$ MeV [Fig. 5(c)] transitions have contributions from the decay of resonance R2 (1^- , 1) and from the direct capture process. On the other hand, both the resonances R2 and R5 (0^- , 1) contribute to the energy variation of $S(E)$ through the $E1$ transition to the second excited state at 3.95 MeV [Fig. 5(b)] and through the $M1$ transition to the fourth excited state at 5.11 MeV [Fig. 5(d)]. The values of $S(E)$ at $E = 0$ corresponding to the four transitions are dominated by the direct capture process, unlike the transition to the ground state

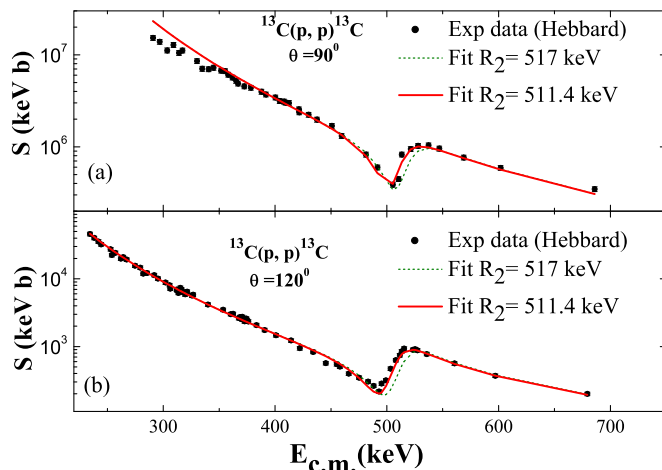


FIG. 3. (Color online) Fits to the elastic scattering data at (a) 90° and (b) 120° . The solid line resulted with the parameters from the fit to Data Set I and the dashed line with parameters from the fit to Data Set II.

of ^{14}N . The direct capture contributions (dotted line) shown in the figures include the external capture component defined by the ANCs of the bound states and the internal capture component through the background poles, if any.

The calculation yielded $S(0) = 0.34 \pm 0.14$ keV b for transition to first excited state (2.31 MeV), with the direct capture component $S^{dc} = 0.17$ keV b, and with the interference contribution $S^{\text{int}} = 0.08$ keV b, respectively.

The direct capture to the second excited state at 3.95 MeV proceeds through $E1$ transition along with $E1$ decay of the resonances R2 and R5. The fit to data for the $R/DC \rightarrow 3.95$ MeV transition [Fig. 5(b)] shows that the interference between the $E1$ amplitudes is destructive in both the low and the high energy tail regions of the resonance R2. The fit resulted

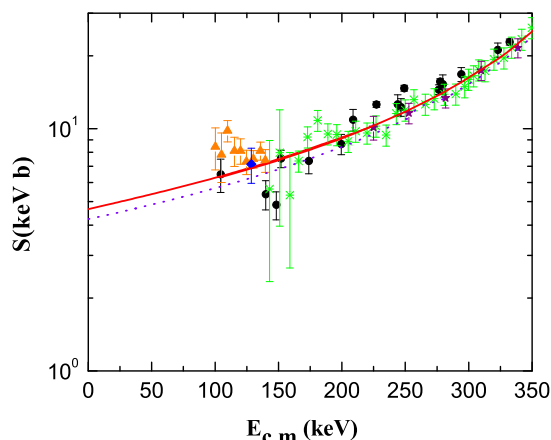


FIG. 4. (Color online) The low energy astrophysical S factor for the $^{13}\text{C}(p,\gamma)^{14}\text{N}_{\text{gs}}$ reaction. The data points are from King *et al.* [6] (black \bullet), Hester *et al.* [10] (blue \diamond), Woodbury *et al.* [7] (orange Δ), Hebbard *et al.* [9] (green \oplus), and Genard *et al.* [11] (violet \star). The solid curve denotes the R -matrix calculation with a parameter set (Set 1) fitting and the dashed curve represents calculation with parameters (Set 2) fitting Data Set II.

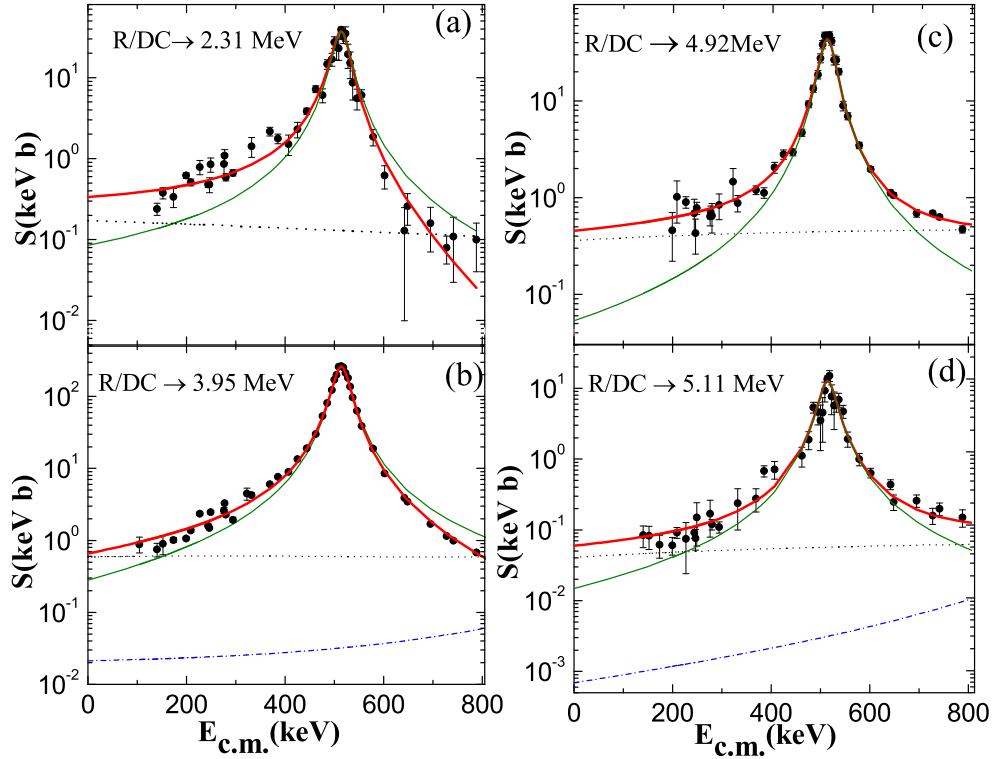


FIG. 5. (Color online) The astrophysical S factors for the captures to the first four excited states of ^{14}N in the $^{13}\text{C}(p,\gamma)^{14}\text{N}$ reaction. The red solid lines in all four panels denote the total S factor from the fits while the green lines represent the contributions of the 1^- resonance state. The dotted lines in the panels are the calculated direct capture contributions to the states. The dashed-dotted lines in the lower panels (b) and (d) show the contributions of the 0^- resonance state in the captures to the second and fourth excited states of ^{14}N .

in total $S(0) = 0.66 \pm 0.17$ keV b with $S^{R^2+R^5}(0) = 0.30$ keV b and the rest coming from the direct capture process and its interference with the resonant term.

The four excited states beyond the the second excited state at 3.95 MeV in the nucleus ^{14}N are positive parity states and

hence the resonant decays from R2 ($1^-, 1$) and R5 ($0^-, 1$) are either $E2$ or $M1$ type.

The data for the $R/DC \rightarrow 4.92$ MeV transition [Fig. 5(c)] have contributions from resonance R2 only and also from the direct capture component. The resultant total $S(0) = 0.45 \pm 0.09$ keV b with $S^{R^2} = 0.06$ keV b and $S^{dc} = 0.36$ keV b.

Both the resonances R2 and R5 can contribute to the transition $R/DC \rightarrow 5.11$ MeV ($2^-, 0$), the fourth excited state of ^{14}N [Fig. 5(d)]. The resonances decay by $E2$ transition to this state. The high energy background poles of 0^- and 1^- spins at 15 MeV also decay by $E2$ transition. Thus, interference is possible between the internal capture amplitude and the resonant amplitude. The direct capture component shows a decreasing trend with energy for this transition. A good overall fit was obtained producing a total $S(0) = 0.059 \pm 0.031$ keV b with the resonant contribution giving $S^{R^2+R^5} = 0.015$ keV b, where R5 has a very small contribution. The direct capture to this state yields $S^{dc} = 0.041$ keV b. The interference contributes only about 5% of the total $S(0)$.

The results of the best fit to the $R/DC \rightarrow 5.69$ MeV state are shown in Fig. 6(a). It includes contributions from the resonances R2 and R5 and the direct capture process. Unlike the fourth excited state, the resonances decay by $M1$ transition to this state. The chosen background poles also decay through $M1$ transition. An excellent fit to the data, at both low and high energy wings of resonance R2, was obtained. The fit yielded a total $S(0) = 0.60 \pm 0.30$ keV b that includes

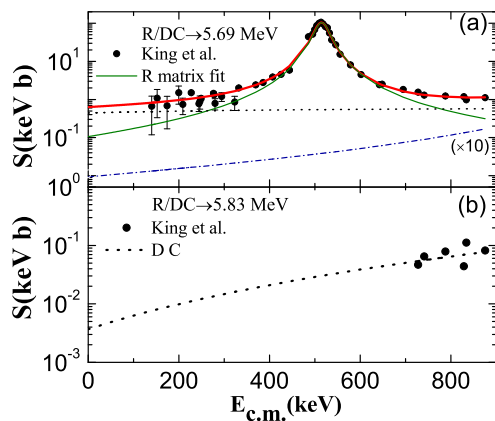


FIG. 6. (Color online) The upper panel (a) shows the S factor for the capture to the fifth excited state ($1^-, 5.69$ MeV) with the corresponding best-fit curve (red solid line). The contributions of the 1^- resonance are given by the green solid curve and of the 0^- resonances by the dashed-dotted curve (multiplied by 10). The direct capture contribution is shown by the dotted curve. The lower panel shows the available data and the fit to it assuming only a direct capture mechanism.

TABLE III. $S(0)$ values for each measured γ transition and the associated uncertainties. Column 4 gives the uncertainty in the individual astrophysical S -factor values arising from the variations in the resonance parameters. The systematic uncertainty of $\sim 11\%$ has been included in column 5. Column 6 lists the uncertainties S_{oth} arising from the ANCs, channel radius, and background pole positions. The last column gives the total uncertainty associated with each $S(0)$.

Data Set	E_x (MeV)	$S(0)$ (keV b)	$\Delta S_{\text{stat}}(0)$ (keV b)	$\Delta S_{\text{sys}}(0)$ (keV b)	$\Delta S_{\text{oth}}(0)$ (keV b)	$\Delta S(0)$ (keV b)
I	0.0	4.72	0.21	0.54	0.63	0.86
	2.31	0.34	0.02	0.04	0.14	0.15
	3.95	0.66	0.02	0.07	0.17	0.19
	4.92	0.45	0.003	0.05	0.09	0.10
	5.11	0.06	0.002	0.007	0.03	0.03
	5.69	0.60	0.003	0.07	0.03	0.31
II	0.0	4.23	0.20	0.48	0.64	0.82

$S^{R2+R5} = 0.11$ keV b and $S^{dc} = 0.44$ keV b. The interference term contributes about 13% to the total $S(0)$.

In Fig. 6(b), the available limited data for the transition to the sixth excited state at 5.84 MeV has been plotted along with the estimated direct capture contribution. A background pole at 15 MeV having spin and parity of 1^- was included in the calculation to account for the internal capture component. With the ANCs taken from the literature [14], the model calculation reproduces the available data at higher energies. The total $S(0)$ obtained from the fit is 0.016 ± 0.002 keV b.

C. Total S factor and the uncertainties

The total astrophysical S factor or $S(E)$ of the $^{13}\text{C}(p, \gamma)^{14}\text{N}$ capture reaction as a function of energy is determined by summing the energy dependences of all the individual $S(E)$ functions for transitions to the ground and the excited states of ^{14}N . Estimated from the extrapolation of the R -matrix fit to Data Set I, the value of $S(0)$ is 6.83 ± 0.95 keV b. The

uncertainty in total $S(0)$ now includes the contribution of systematic error of 11.3%. The value compares well with 7.0 ± 1.5 keV b given in the NACRE compilation [5] but is lower than $8.1^{+1.2}_{-1.1}$ keV b used in NACRE II [29]. Without the data for the primary decays to the excited states, the fitting of Data Set II yields 4.23 ± 0.82 keV b for transition to the ground state only, and the value compares well with the value obtained for Data Set I.

Table III displays the uncertainties associated with individual contributions to the total S -factor value at $E = 0$. In column 3 of the table, the final $S(0)$ estimates of the transitions have been listed. The uncertainty estimate routine MINOS has been utilized for the uncertainty analysis of the parameters, shown in column 4 of Table III. In the uncertainty analysis, a simultaneous fit was carried out with the primary decay data of Ref. [6] and the scattering data of Ref. [9]. For a multiparameter fit, a value of $\Delta\chi^2 = 18.1$ was used considering 16 free R -matrix fit parameters in the relation $\chi^2 = \chi_{\text{min}}^2 + \Delta\chi^2$ (see Ref. [28]). The resultant uncertainty in the parameters (Table III) reflects the statistical uncertainty in the extrapolation. In column 5, systematic uncertainties of 11.3% [6] in the absolute values are listed. Column 6 displays the uncertainties associated with each extrapolated $S(0)$ value coming from the variations in the respective ANC (ΔS_{ANC}), channel radius r_c (ΔS_{rc}), and the locations of the background poles (ΔS_{bg}). The uncertainty ΔS_{ANC} of the $S(0)$ of each transition has been estimated from the limits of the individual ANC value given Table I. The component ΔS_{rc} has been determined by varying the channel radius value with the condition of $\chi^2 = \chi_{\text{min}}^2 + 1$ for each transition. However, the contribution of ΔS_{bg} is obtained by introducing a 20 MeV shift in the background pole position. All three contributions have been added in quadrature to produce the uncertainty term ΔS_{oth} listed in column 6 of Table III. The total uncertainty $\Delta S(0)$ of an individual transition includes the contributions of columns 4, 5, and 6 added in quadrature. The overall uncertainty in the extrapolated total $S(0)$, the sum of the uncertainties associated with all individual decays of Data Set I, is about 14.0%. With Genard's data in Data Set II, the estimated uncertainty in $S(0)$

TABLE IV. Low temperature reaction rates using the extrapolated S -factor values from the present analysis. The reaction rate is given in $\text{cm}^3 \text{mole}^{-1} \text{s}^{-1}$. The ‘Low’ and ‘High’ denote the lower and upper limits of uncertainty in the adopted reaction rate.

T_9	Low	Reaction rate	High	T_9	Low	Reaction rate	High
0.001	2.21×10^{-50}	2.55×10^{-50}	2.9×10^{-50}	0.06	3.92×10^{-07}	4.53×10^{-07}	5.14×10^{-07}
0.002	2.74×10^{-38}	3.17×10^{-38}	3.6×10^{-38}	0.07	2.09×10^{-06}	2.41×10^{-06}	2.74×10^{-06}
0.003	2.0×10^{-38}	2.32×10^{-38}	2.63×10^{-38}	0.08	8.32×10^{-06}	9.62×10^{-06}	1.09×10^{-05}
0.004	9.98×10^{-29}	1.15×10^{-28}	1.31×10^{-28}	0.09	2.67×10^{-05}	3.09×10^{-05}	3.51×10^{-05}
0.005	4.24×10^{-26}	4.9×10^{-26}	5.56×10^{-26}	0.1	7.33×10^{-05}	8.47×10^{-05}	9.62×10^{-05}
0.006	4.27×10^{-24}	4.94×10^{-24}	5.61×10^{-24}	0.2	0.02	0.029	0.03
0.007	1.7×10^{-22}	1.96×10^{-22}	2.23×10^{-22}	0.3	0.51	0.59	0.67
0.008	3.54×10^{-21}	4.09×10^{-21}	4.65×10^{-21}	0.4	5.18	5.99	6.80
0.009	4.61×10^{-20}	5.33×10^{-20}	6.05×10^{-20}	0.5	36.18	41.82	47.47
0.01	4.2×10^{-19}	4.85×10^{-19}	5.51×10^{-19}	0.6	156.91	181.39	205.88
0.02	1.37×10^{-13}	1.59×10^{-13}	1.8×10^{-13}	0.7	462.84	535.07	607.31
0.03	6.42×10^{-11}	7.42×10^{-11}	8.42×10^{-11}	0.8	1041.25	1203.75	1366.26
0.04	3.073×10^{-09}	3.56×10^{-09}	4.04×10^{-09}	0.9	1939.53	2242.23	2544.93
0.05	4.81×10^{-08}	5.56×10^{-08}	6.32×10^{-08}	1	3158.3	3651.21	4144.13

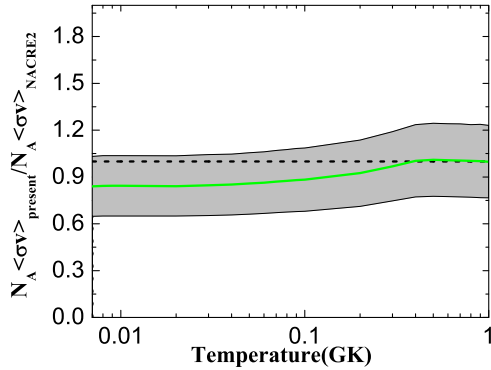


FIG. 7. (Color online) Reaction rate ratio of the present reaction rate to the rate compiled in NACRE II [29] as a function of temperature for the $^{13}\text{C}(p,\gamma)^{14}\text{N}$ capture reaction. The shaded region corresponds to estimated uncertainties of the S -factor values.

for ground state transition is now 19.4%, whereas with King's data the uncertainty associated with the extrapolated S factor for the ground state transition is around 18.2%.

D. Nuclear reaction rate

The thermonuclear reaction rate $N_A \langle\sigma v\rangle$ for $^{13}\text{C}(p,\gamma)^{14}\text{N}$ is estimated using the expression

$$N_A \langle\sigma v\rangle = 3.7318 \times 10^{10} \mu^{1/2} (T_9)^{-3/2} \times \int_0^\infty dE E \sigma \exp[-11.605E/T_9], \quad (2)$$

where N_A is the Avogadro number, μ the reduced mass of the colliding nuclei, T_9 is the stellar temperature in GK, E the energy in the center of mass and $\sigma(E)$ is the cross section in barns. The numerical integration was carried out by the code AZURE2. Table IV lists the calculated reaction rates along with the lower and the upper limits for $T_9 = 0.001$ to $T_9 = 1.0$. In Fig. 7, the reaction rates from the present analysis have been plotted relative to the tabulated reaction rates of $^{13}\text{C}(p,\gamma)^{14}\text{N}$ from the NACRE II compilation [29] over the same temperature range. The uncertainty band shown in the figure corresponds to all the uncertainties included in the estimation of the total $S(0)$ shown in Table III. In the temperature range below $T_9 = 0.1$ which defines the hydrostatic burning phase, the reaction rates from the present calculation are about 10–15% lower than the values of NACRE II but compare well with adopted values of NACRE I [5]. On the other hand, beyond $T_9 = 0.1$, a temperature range relevant to hydrogen burning in red giants and AGB stars, the reaction rates from the present work agree well with the adopted values in NACRE II.

IV. SUMMARY AND CONCLUSION

We presented a reanalysis of a simultaneous fit to the experimental data for the capture reaction $^{13}\text{C}(p,\gamma)^{14}\text{N}$ from Refs. [6,11,15] and the scattering data for $^{13}\text{C}(p,p_0)^{13}\text{C}$ from Ref. [9] within the R -matrix framework using the code AZURE2. Two different data sets, Data Sets I and II, were prepared based on the measurements of King *et al.* [6] and Genard *et al.* [11] for the reaction $^{13}\text{C}(p,\gamma)^{14}\text{N}_{gs}$ populating the resonance state around 8.06 MeV excitation. Subsequently, R -matrix analyses were performed for both the data sets separately. The astrophysical S factor at zero energy, $S(0)$, was derived through extrapolation for the two data sets. For the transition to the ground state of ^{14}N , the present analysis, with the data from [6], yielded $S(0) = 4.72 \pm 0.86$ keV b which is lower than $S(0) = 5.16 \pm 0.72$ keV b reported in Ref. [14] from their R -matrix fit to the same data. The values, however, are consistent within the error bars. Analysis with the ground state transition data of [11] resulted in a $S(0) = 4.23 \pm 0.82$ keV b, a value higher than that obtained by Genard *et al.* Excellent agreement is obtained between the resultant $S(0)$ values, determined with two different data sets for the ground state transition from the 1^- resonance of ^{14}N . Inclusion of the contributions of transitions to the excited states, from the measurement of King *et al.*, produced a total $S(0) = 6.83 \pm 0.95$ keV b and $S(25 \text{ keV}) = 7.10 \pm 1.1$ keV b at $E_{c.m.} = 25$ keV for the $^{13}\text{C}(p,\gamma)^{14}\text{N}$ capture. The values are lower than the total $S(0) = 7.6 \pm 1.10$ keV b and $S(25 \text{ keV}) = 8.0 \pm 1.2$ keV b of [14]. However, the error bars of the two estimates overlap.

The simultaneous analysis including the elastic scattering data indicates that the position of the 1^- , $T = 1$ resonance state in ^{14}N is at $E_x = 8062.0 \pm 3.0$ keV rather than 8068.1 ± 0.5 keV [6]. This is probably the main cause for the inconsistencies in the values of $S(0)$ and $S(25 \text{ keV})$ from the two data sets. The precise energy of the 1^- level must be determined accurately. Also, inclusion of the higher energy data further constrains the energy dependence of the cross section allowed by the R -matrix model at low energy, improving the uncertainty in the extrapolation. Note that the data of King *et al.*, which extend up to $E_{c.m.} \approx 100$ keV, have significant scattering in the data points at lower energies. On the other hand, the measurement of Genard *et al.* has much less scattering in the low energy region but the data extend only up to $E_{c.m.} \approx 220$ keV. Hence, a further measurement with precision to reduce the uncertainty in and scattering of the data points at low energies extending even beyond 100 keV is definitely worthwhile.

ACKNOWLEDGMENTS

R.D. acknowledges support from the National Science Foundation through Grant No. PHY-1068192 and the Joint Institute for Nuclear Astrophysics Grant No. PHY08-22648.

[1] C. Rolfs and W. S. Rodney, *Cauldrons in the Cosmos* (University of Chicago Press, Chicago, 1988).

[2] M. Lugaro, F. Herwig, J. C. Lattanzio, R. Gallino, and O. Straniero, *Astrophys. J.* **586**, 1305 (2003).

- [3] C. Iliadis, *Nuclear Physics in Stars* (Wiley-VCH, Weinheim, 2007).
- [4] E. W. Kolb and M. S. Turner, *The Early Universe* (Addison-Wesley, Reading, 1990).
- [5] C. Angulo, M. Arnould, M. Rayet, P. Descouvemont *et al.*, *Nucl. Phys. A* **656**, 3 (1999).
- [6] J. D. King, R. E. Azuma, J. B. Vise, J. Görres, C. Rolfs, H. P. Trautvetter, and A. E. Vlieks, *Nucl. Phys. A* **567**, 354 (1994).
- [7] E. J. Woodbury and W. A. Fowler, *Phys. Rev.* **85**, 51 (1952).
- [8] J. D. Seagrave, *Phys. Rev.* **85**, 197 (1952).
- [9] D. F. Hebbard and J. L. Vogl, *Nucl. Phys.* **21**, 652 (1960).
- [10] R. E. Hester and W. A. S. Lamb, *Phys. Rev.* **121**, 584 (1961).
- [11] G. Genard, P. Descouvemont, and G. Terwagne, *J. Phys. Conf. Ser.* **202**, 012015 (2010).
- [12] F. Ajzenberg-Selove, *Nucl. Phys. A* **449**, 1 (1986).
- [13] G. R. Caughlan and W. A. Fowler, *At. Data Nucl. Data Tables* **40**, 283 (1988).
- [14] A. M. Mukhamedzanov, A. Azhari, V. Burjan, C. A. Gagliardi, V. Kroha, A. Sattarov, X. Tang, L. Trache, and R. E. Tribble, *Nucl. Phys. A* **725**, 279 (2003).
- [15] V. J. Zeps, E. G. Adelberger, A. Garcia, C. A. Gossett, H. E. Swanson, W. Haeberli, P. A. Quin, and J. Sromicki, *Phys. Rev. C* **51**, 1494 (1995).
- [16] R. E. Azuma, E. Uberseder, E. C. Simpson, C. R. Brune *et al.*, *Phys. Rev. C* **81**, 045805 (2010).
- [17] C. R. Brune, *Phys. Rev. C* **66**, 044611 (2002).
- [18] F. Ajzenberg-Selove, *Nucl. Phys. A* **523**, 1 (1991).
- [19] J. D. King, *Can J. Phys.* **69**, 828 (1991).
- [20] <https://www-nds.iaea.org/exfor/exfor.htm>.
- [21] P. Descouvemont and D. Baye, *Rep. Prog. Phys.* **73**, 036301 (2010).
- [22] F. C. Barker and T. Kajino, *Aust. J. Phys.* **44**, 369 (1991).
- [23] C. Angulo and P. Descouvemont, *Nucl. Phys. A* **690**, 755 (2001).
- [24] C. Iliadis, J. DAuria, S. Starrfield, W. J. Thompson, and M. Wiescher, *Astrophys. J. Suppl.* **134**, 151 (2001).
- [25] A. Kontos, J. Görres, A. Best, M. Couder *et al.*, *Phys. Rev. C* **86**, 055801 (2012).
- [26] L. Trache, A. Azhari, H. L. Clark, C. A. Gagliardi, Y.-W. Lui, A. M. Mukhamedzhanov, R. E. Tribble, and F. Carstoiu, *Phys. Rev. C* **58**, 2715 (1998).
- [27] P. Bem, V. Burjan, V. Kroha, J. Novak, S. Piskor, E. Simeckova, J. Vincour, C. A. Gagliardi, A. M. Mukhamedzhanov, and R. E. Tribble, *Phys. Rev. C* **62**, 024320 (2000).
- [28] P. Descouvemont, A. Adahchour, C. Angulo, A. Coc, and E. Vangioni-Flam, *At. Data Nucl. Data Tables* **88**, 203 (2004).
- [29] Y. Xu, K. Takahashi, S. Goreily, M. Arnould *et al.*, *Nucl. Phys. A* **918**, 61 (2013).